









RESEARCH ARTICLE

ATR-FTIR spectrum analysis of plasma samples for rapid identification of recovered COVID-19 individuals

Boris Y. Karas¹ | Vera E. Sitnikova¹  | Tatiana N. Nosenko¹  |
Vladimir G. Dedkov^{2,3}  | Natalia A. Arsentieva²  | Natalia V. Gavrilenko⁴ |
Ivan S. Moiseev⁴  | Areg A. Totolian²  | Andrey V. Kajava⁵  |
Mayya V. Uspenskaya¹ 

¹Institute BioEngineering, ITMO University, St. Petersburg, Russia

²Saint-Petersburg Pasteur Institute, Federal Service on Consumers' Rights Protection and Human Well-Being Surveillance, St. Petersburg, Russia

³Martinsonsky Institute of Medical Parasitology, Tropical and Vector Borne Diseases, Sechenov First Moscow State Medical University, Moscow, Russia

⁴Raisa Gorbacheva memorial Research Institute for Pediatric Oncology, Hematology and Transplantation, Pavlov First Saint Petersburg State Medical University, St. Petersburg, Russia

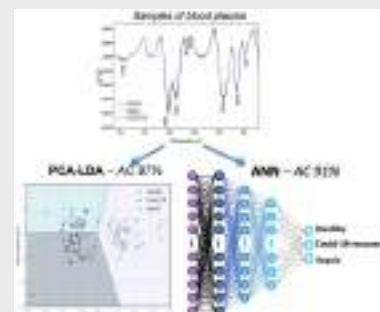
⁵Centre de Recherche en Biologie cellulaire de Montpellier, Université Montpellier, Montpellier, France

Correspondence

Vera E. Sitnikova, Institute
BioEngineering, ITMO University,
St. Petersburg 197101, Russia.
Email: v.e.sitnikova@gmail.com

Abstract

The development of fast, cheap and reliable methods to determine seroconversion against infectious agents is of great practical importance. In the context of the COVID-19 pandemic, an important issue is to study the rate of formation of the immune layer in the population of different regions, as well as the study of the formation of post-vaccination immunity in individuals after vaccination. Currently, the main method for this kind of research is enzyme immunoassay (ELISA, enzyme-linked immunosorbent assay). This technique is sufficiently sensitive and specific, but it requires significant time and material costs. We investigated the applicability of attenuated total reflection (ATR) Fourier transform infrared (FTIR) spectroscopy associated with machine learning in blood plasma to detect seroconversion against SARS-CoV-2. The study included samples of 60 patients. Clear spectral differences in plasma samples from recovered COVID-19 patients and conditionally healthy donors were identified using multivariate and statistical analysis. The results showed that ATR-FTIR spectroscopy, combined with principal components analysis (PCA) and linear discriminant analysis (LDA) or artificial neural network (ANN), made it possible



Abbreviations: Ab, antibody; ANN, artificial neural networks;

ATR-FTIR, attenuated total reflection–Fourier transform infrared spectroscopy; IgG, immunoglobulin G; PCA-LDA, principal component analysis–linear discriminant analysis.

to efficiently identify specimens from recovered COVID-19 patients. We built classification models based on PCA associated with LDA and ANN. Our analysis led to 87% accuracy for PCA-LDA model and 91% accuracy for ANN, respectively. Based on this proof-of-concept study, we believe this method could offer a simple, label-free, cost-effective tool for detecting seroconversion against SARS-CoV-2. This approach could be used as an alternative to ELISA.

KEYWORDS

ANN, ATR-FTIR spectroscopy, chemometric, COVID-19, PCA-LDA, plasma, sepsis

1 | INTRODUCTION

More than one and a half years have passed since the beginning of the COVID-19 epidemic that arose at the end of December 2019 in Wuhan, Hubei province (China). During this time, the epidemic turned into a pandemic and covered all continents, except for Antarctica. By May 31, 2021, the cumulative number of cases reported globally by August 17, 2021 is now over 206 million and the cumulative number of deaths is almost 4.4 million [1].

The COVID-19 epidemic has brought dramatic changes to humanity's lifestyles and caused enormous economic harm. The etiological agent of the disease is the previously unknown beta-coronavirus SARS-CoV-2, which was detected in biological samples from patients with severe pneumonia in the Chinese city of Wuhan in December 2019. SARS-CoV-2 belongs to the sarbecovirus subgenus and is the seventh known coronavirus capable of infecting humans [2].

COVID-19 is characterized by different variants of the course of the disease, from asymptomatic carriage to severe forms of pneumonia with the development of respiratory distress syndrome and "cytokine storm" [3]. The absence of symptoms significantly complicates the identification of infection, as well as understanding which part of the population has already been ill and carries the risk of spreading the infection [4–7].

To meet the needs for laboratory diagnostics of COVID-19 in different countries, a large number of diagnostic tests have been developed in a short time. At the same time, first of all, tests were developed to detect the disease in the acute phase. As a rule, these were molecular techniques based on reverse transcription polymerase chain reaction (RT-qPCR) [8–10] or based on isothermal amplification (RT-LAMP) [11], as well as RDT (rapid diagnostic tests) based on lateral immunochromatography to detect the SARS-CoV-2 antigen [12, 13]. Such diagnostic techniques make it possible to detect the disease at an early stage, which is

important both from the point of view of diagnosis and from the point of view of organizing anti-epidemic measures.

In addition, to assess the presence of immune responses, both during illness and after clinical recovery, many tests have been developed to detect immunoglobulins of various classes against the SARS-CoV-2 virus. These tests are implemented mainly in the ELISA format and are widely used at present [14]. Given the fact that a significant part of the population has already been ill with COVID-19, or has been vaccinated, there are problems associated with assessing population immunity, its dynamics, evaluating the effectiveness of post-vaccination immunity, etc. To solve these problems, it is necessary to conduct large-scale research, which requires the involvement of significant material and human resources. Therefore, the development of alternative methods of mass testing for the presence of seroconversion to SARS-CoV-2 is an urgent task.

There are many attempts to apply Fourier transform infrared spectroscopy (FTIR) as a fast, reliable and affordable screening for a variety of diseases. FTIR spectroscopy, combined with various data processing techniques, has been widely used in many cancer research [15–17]. Nowadays, modern computing tools make it possible to process huge amounts of information in a matter of minutes. The use of machine learning and chemometric methods in the processing of medical data allows you to obtain important information without significant costs and resource use.

Attenuated total reflectance FTIR (ATR) spectroscopy represents a complementary approach for clinical applications [18] over other infrared approaches [19]. This mode gives high-quality results with better spectral reproducibility when using liquid samples [20]. Thus, ATR-FTIR spectroscopy of biological fluids has attracted a lot of attention from the scientific community for the rapid detection of various health conditions. Zhang et al. [21] showed that ATR-FTIR spectroscopy can be a primary diagnostic tool for patients in the acute phase COVID-19

as a supplement to in-use techniques. The paper [22] shows the potential of ATR-FTIR to classify the severity of COVID-19 disease depending on concomitant diseases. In addition, chemometric processing methods in combination with ATR-FTIR are used to develop diagnostic methods based on the detection of biological markers of the virus in saliva [23, 24, 25, 26]. The sensitivity, specificity and accuracy of the developed models based on FTIR and Raman spectral data for determining the presence of the SARS-CoV-2 virus and determining the severity of COVID-19 disease is very promising.

However, due to the fact that viral samples are rapidly degraded in blood and saliva samples, the application of ATR-FTIR spectroscopy to the analysis of viral samples in a viral transport medium is an extremely relevant research. In [27] FTIR spectroscopy was proposed as a fast and reagent-free screening method for the detection of SARS-CoV-2 in RNA extracts. Using the multivariate analysis of IR spectra, the authors managed to achieve the accuracy, sensitivity, and specificity of the analysis of 97.8%, 97%, and 98.3%, respectively, while testing time after RNA isolation was reduced from hours to minutes.

The article [28] investigated the immunological response to the SARS-Cov-2 vaccine using IR spectroscopy. This research aimed to analyze and compare FTIR spectra of vaccinated people with a positive or negative real-time quantitative RT-qPCR test, evaluating the immunoglobulin and cytokine content as an immunological response through FTIR spectroscopy. The work shows that it was possible to detect biochemical changes through FTIR spectroscopy associated with COVID-19 immune response in vaccinated people, once IgG, IgA, IgM, as well as different cytokines, such as IFN- γ , TNF- α , IL-1 β , IL-6 and IL-10, were detected.

In our article, we talk about the developed method for the rapid detection of recovered COVID-19 patients using IR spectroscopy. The spectral differences between COVID-19 and healthy controls and the potential spectral markers were identified by multivariate and statistical analysis.

2 | EXPERIMENTAL SECTION

2.1 | Sample collection

The work was carried out as part of a project to assess population immunity to SARS-CoV-2 in the population of the Russian Federation, considering the protocol recommended by the WHO. The study was conducted according to the guidelines of the Declaration of Helsinki and approved by the Institutional Ethics Committee of St. Petersburg Pasteur Institute (protocol No 64, May 26, 2020). Before the start of the study, all participants or their legal representatives

familiarized themselves with the purpose and methodology of the study and signed an informed consent. The selection of volunteers for the study was carried out by the method of questionnaires and random sampling [29].

2.2 | Sample preparation and ATR-FTIR spectroscopy

Volunteers' blood samples were taken into vacutainers with EDTA and processed by centrifugation (3000g for 10 min). Plasma was separated from cellular elements, transferred into plastic tubes, and stored at -80°C until analysis. The content of antibodies to SARS-CoV-2 was determined using the Enzyme immunoassay for the determination of IgG antibodies to SARS-Coronavirus 2 in human serum and plasma GA CoV-2 IgG (GA generic assay GmbH, Germany). The results were taken into account by a qualitative method and were considered positive if the cut-off level was exceeded. To study the method of IR spectroscopy have been selected for "IgG⁺" 30 samples from volunteers who recover COVID-19, and 30 samples from "IgG⁻" volunteers without a history COVID-19. In addition, to assess the specificity of the developed technique in relation to the systemic inflammatory response, 40 plasma samples from persons with sepsis as complications of the treatment of oncohematological diseases, collected in 2016–2018, were also studied. Samples were used that were obtained within the interval of 0–3 days from the diagnosis of sepsis. The diagnosis was established based on bacteriological confirmation of bacteremia and clinical diagnosis of sepsis in accordance with the International Guidelines for Management of Sepsis and Septic Shock 2016 [30].

Before the measurements of the plasma, samples were thawed at 25°C . Each sample was measured three times on a Bruker Tensor 37 FTIR spectrometer using an ATR attachment with a diamond-coated zinc selenide crystal with a resolution of 2 cm^{-1} . Thirty-two scans were accumulated per spectrum. The ATR detection crystal was cleaned with 96% v/v ethanol and background spectra were acquired before every acquisition. For each measurement, an aliquot of 10 μL plasma sample was transferred onto the ATR crystal and allowed to dry under mild airflow at room temperature. It took about 10 min for the samples to dry completely. The thickness of the dried blood plasma sample on the ATR crystal was approximately 20 micrometers. The spectra were recorded in the range from 4000 to 600 cm^{-1} .

2.3 | Multivariate and statistical analysis

The measurements were performed in triplicate for each sample and each replicate was included in ML algorithms.

Before analyzing the data, the baseline was corrected for the raw spectral data using the concave rubberband procedure in the OPUS software. Then all spectra were vector normalized. The second derivative of infrared spectra was calculated from the normalized non-smoothed spectra (Figure S1). The spectral region of second derivative of FTIR spectra 1700–900 cm^{-1} was chosen and cross-validation performed using the LOOCV algorithm. In all cases, Savitzky–Golay smoothing (smoothing point 13) (Figure S2), with standard normal variate normalization and mean centering were used for preprocessing. The data were organized in such a way that the samples were divided into training (65%) and test (35%) sets.

Statistical processing of the spectra was carried out in the OriginPro 2019 program using the one-way analysis of variance (ANOVA) followed by Tukey post hoc test was conducted to verify the significance of the selected spectral markers. The data are expressed as means with standard deviations (SD). The level of statistical significance considered $p < 0.05$. Data analysis was performed in The Unscrambler 9.7 (CAMO software) and Python environment using Scikit-learn library [31, 32].

Several algorithms for feature extraction/selection and classification were tested to distinguish samples from healthy donors, COVID-recovered, and patients with sepsis. In order to effectively combat the “The Curse of

Dimensionality” [32, 33, 34], principal component analysis was used as input variables for algorithms: linear discriminant analysis (LDA), support vector machines (SVM) and the K-nearest neighbors method, multi-layer perceptron classifier (MLP), random forest classifier, AdaBoost classifier.

2.4 | Quality performance

The accuracy, sensitivity, specificity, F-score and G-score were calculated in the test set to evaluate the model's classification performances. The accuracy represents the total number of samples correctly classified considering true and false negatives. The sensitivity is the proportion of positive samples (i.e., covered COVID-19 or patients with sepsis) correctly classified. The specificity represents the proportion of negative samples (i.e., healthy uninfected controls) correctly classified. The F-score measures the overall classification performance considering imbalanced data, and the G-score measures the overall classification performance not accounting for class sizes [35]. The equations to calculate these parameters are shown in Table 1.

3 | RESULTS AND DISCUSSION

3.1 | Comparison of blood plasma from recovered COVID-19 patients with control plasma samples

Blood plasma consists of more than 90% by volume of water. It is known that plasma consists of proteins (including fibrinogen), cholesterol, glucose, urea, triglycerides and other more dilute compounds, all of which can be recorded in spectra. However, only components with a higher content can be identified in the spectra and

TABLE 1 Equations to calculate the classification quality parameters.

Parameter	Equation
Accuracy (AC) (%)	$\frac{TP+TN}{TP+FP+TN+FN} \times 100$
Sensitivity (SENS) (recall) (%)	$\frac{TP}{TP+FN} \times 100$
Specificity (SPEC) (precision) (%)	$\frac{TN}{TN+FP} \times 100$
F-score (%)	$\frac{2 \times \text{SENS} \times \text{SPEC}}{\text{SENS} + \text{SPEC}}$
G-score (%)	$\sqrt{\text{SENS} + \text{SPEC}}$

Abbreviations: FN, negative; FP, positive; TN, negative; TP, true positive.



FIGURE 1 Average IR spectra of the blood plasma group with antibodies to SARS-CoV-2 (IgG⁺) and without antibodies to SARS-CoV-2 (IgG⁻) and their standard deviation.

provide useful information. To obtain better FTIR spectra of the dissolved proteins and other components, plasma samples have been dried on ATR crystal.

Averaged spectra minimize the effect of individual differences and are therefore more representative. Figure 1 shows the averaged (pre-processed) FTIR spectra of plasma samples from groups with antibodies to SARS-CoV-2 (IgG^+) and without antibodies (IgG^-), which are very similar overall and comparable to previous reports of FTIR of plasma and serum [36, 37]. The spectra are very similar compared to other plasma samples reported and

discussed before in the literature. Therefore, the wave-number assignment has been adapted from previous studies (Table 2) [38].

The average spectra from both donors' groups appear very similar, thus, for a more detailed consideration of the differences, difference spectra are usually calculated. Figure 2 shows the difference spectrum that was obtained by subtracting the average IR spectrum of the SARS-CoV-2 antibody group (IgG^+ -group) from the average spectrum of the SARS-CoV-2 antibody-free group (IgG^- -group). The area of the graph above zero shows

TABLE 2 Band assignments and statistical comparisons between recovered COVID-19 patients and control spectra in band locations and relative absorbance.

Absorption band position (cm^{-1})				Intensity		
Absorption band	Control	Recovered COVID-19 patients	<i>p</i>	Control	Recovered COVID-19 patients	<i>p</i>
—OH	3340	3340.42 ± 2.17	3338.48 ± 10.07	0.043 ± 0.002	0.048 ± 0.002	**
Amide A	3288	3284.96 ± 1.34	3285.11 ± 0.91	0.045 ± 0.002	0.048 ± 0.001	**
$\nu_{\text{as}}(\text{CH}_3)$	2958	2957.38 ± 0.53	2957.23 ± 0.48	0.015 ± 0.001	0.015 ± 0.01	
$\nu_{\text{as}}(\text{CH}_2)$	2926	2928.15 ± 0.90	2927.75 ± 1.29	0.018 ± 0.002	0.018 ± 0.02	
$\nu_{\text{s}}(\text{CH}_3)$	2874	2871.28 ± 0.47	2871.37 ± 0.48	$0.0089 \pm 6\text{E-}4$	$0.0088 \pm 5\text{E-}4$	
Amide I	1645	1643.61 ± 1.81	1643.58 ± 2.21	0.053 ± 0.001	0.052 ± 0.001	**
C=O	1745	1738.85 ± 2.42	1739.95 ± 2.88	$8.5\text{E-}4 \pm 4\text{E-}4$	$0.0011 \pm 5\text{E-}4$	*
Amide II	1536	1537.34 ± 0.56	1538.04 ± 1.05	0.063 ± 0.00277	0.066 ± 0.018	*
$\delta(\text{CH}_2)$	1452	1452.96 ± 0.56	1452.58 ± 1.29	$0.0181 \pm 9\text{E-}4$	$0.0177 \pm 9\text{E-}4$	*
$\nu_{\text{s}}(\text{COO}^-)$	1399	1399.93 ± 0.58	1400.37 ± 0.40	0.023 ± 0.001	$0.0237 \pm 9\text{E-}4$	
$\nu_{\text{as}}(\text{PO}_2^-)$	1241	1241.07 ± 1.46	1240.52 ± 1.64	$0.0105 \pm 7\text{E-}4$	$0.0102 \pm 5\text{E-}4$	*
Amide III	1311	1311.80 ± 1.00	1312.81 ± 1.08	$0.0091 \pm 7\text{E-}4$	$0.0088 \pm 6\text{E-}4$	
$\nu_{\text{s}}(\text{C—O—C})$	1170	1170.71 ± 0.66	1170.50 ± 1.75	$0.0020 \pm 3\text{E-}4$	$0.0019 \pm 2\text{E-}4$	
$\nu_{\text{s}}(\text{PO}_2^-)$	1078	1078.67 ± 0.57	1078.32 ± 0.77	$0.0063 \pm 5\text{E-}4$	$0.0054 \pm 3\text{E-}4$	*
C—O	1029	1029 ± 0.24	1029 ± 0.20	$0.0042 \pm 4\text{E-}4$	$0.0041 \pm 4\text{E-}4$	*

Note: All centered bands existed in all measured spectra. Data are in mean (standard deviation).

* $p < 0.05$; ** $p < 0.01$; *** $p < 0.001$.

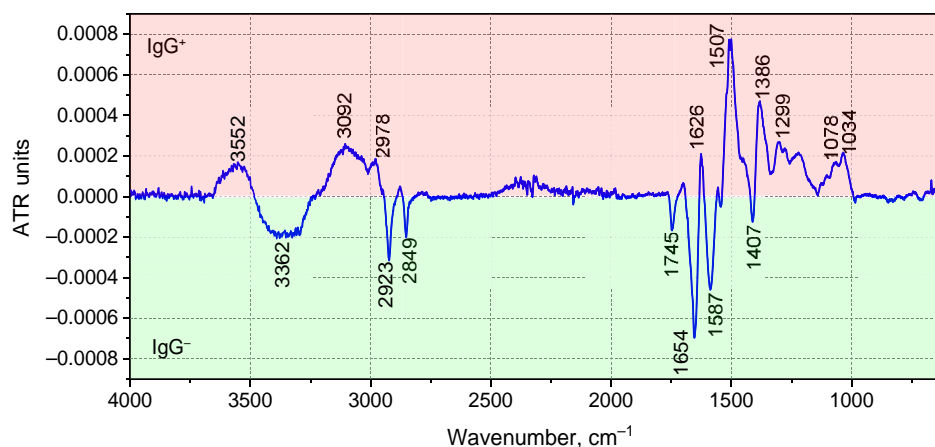


FIGURE 2 Difference FTIR spectrum (the result of subtracting the average IgG^+ -group spectrum from the average IgG^- -group spectrum).

those components of the IR spectrum, which were more in the IgG⁻-group, and the area of the graph below zero shows the components of the IR spectrum, which are more in the IgG⁺-group. Hence, it can be seen that the average spectra of the two groups differ both in the lipid regions (2923, 2849 and 1745 cm⁻¹) and in the protein and carbohydrate regions of the spectrum. The IgG⁺- group is characterized by a greater contribution of frequencies of 1654 (α-helical conformations of proteins) and 1587 cm⁻¹ (fibrinogen). The IgG⁻-group is characterized by a greater absorption at a wavenumber of 1626 cm⁻¹ (β-sheet conformations of protein), a greater absorption of the Amide II band and carbohydrate bands of the spectrum (1070–1030 cm⁻¹).

When analyzing the original IR spectra using ANOVA, it was found that some bands had significant changes in intensity in the group of recovered COVID-19 patients (Table 2), which indicates changes in the amount of some components of blood plasma. As can be seen from Table 2 and Table S1, the values of the relative absorbance and the wave number of the protein absorption bands of both amide A and amide III showed significant differences between the samples with recovered COVID-19 patients and the control group ($p < 0.05$), which indicates changes in protein concentrations.

Standard procedure signal amplification in the spectra is the calculation of the second derivative. This technique helps to conduct a more detailed analysis, by the removal of a wide base of artifacts and sharpening. Figure 3 shows the averaged second derivatives of IR spectra for two groups of donors with standard deviations.

ANOVA (Table 2) shows that the differences in the frequencies of stretching vibrations of CH₂ and CH₃ groups are not statistically significant for the two groups of donors.

The average second derivatives of the IR spectra (Table S1) demonstrate changes in the intensity of the 1399 cm⁻¹ band, which is associated with symmetric stretching of COO⁻ in the side chains of the protein.

There is a significant change ($p < 0.01$) in the absorption of this band in the recovered COVID-19 patient group, without a band shift.

The authors of Reference [21], who studied the IR spectra of blood plasma of patients with COVID-19 in the acute phase, found significant differences in the lipid regions of the spectrum at frequencies of 1242 and 1078 cm⁻¹. The bands centered at 1242 and 1078 cm⁻¹ correspond to asymmetric and symmetric regions of PO₂⁻ groups, respectively [38]. Functional group PO₂⁻ may arise from nucleic acids or phospholipids in the blood serum. Since nucleic acids such as extracellular circulating DNA (cirDNA) [39] or SARS-CoV-2 RNA [40] are found in a limited amount in human serum, the band at 1078 cm⁻¹ can be attributed to phospholipids. The authors of Reference [41] confirm that in patients with mild, severe and fatal COVID-19, sphingolipids and lysolecithin were observed with an increase of 3.5–5.5 times, while lecithin decreased by 50%–80%. However, such differences are not typical for the groups of healthy donors and recovered COVID-19 patients.

As can be seen from Tables 2 and S1, the differences between the groups of healthy donors and recovered COVID-19 patients, which have statistically significant differences, concern only the protein ranges of the spectrum.

Thus, for further multivariate statistical analysis, the optimal spectrum range of 1680–1489 cm⁻¹ was selected, which characterizes the protein part of the spectrum, since changes occur in the protein composition of blood plasma.

3.2 | Principal components analysis of recovered COVID-19 patients and control plasma samples

For antibody against SARS-CoV-2 determination, unsupervised clustering was applied to the FTIR spectra of the

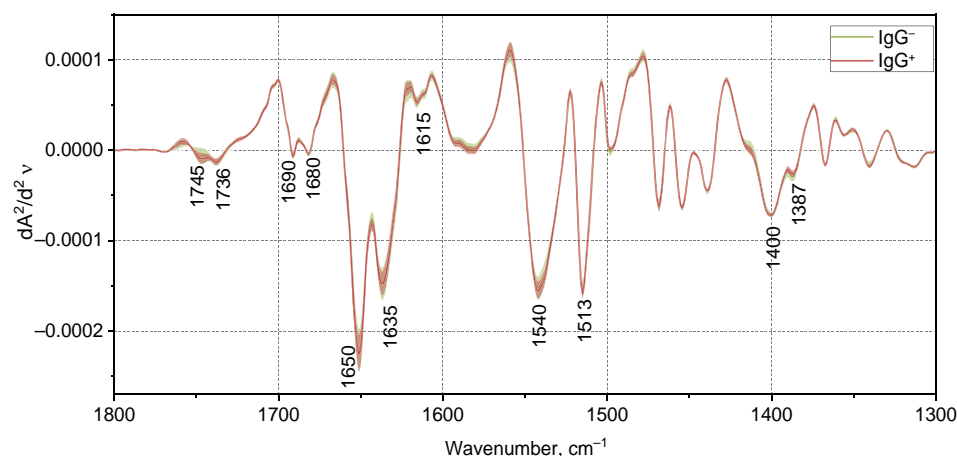


FIGURE 3 Average second derivatives of vector normalized IR spectra of blood plasma samples with antibodies to SARS-CoV-2 (IgG⁺) and without antibodies (IgG⁻) and their standard deviation.

recovered COVID-19 patients and the control group using principal component analysis (PCA). The accuracy of clustering was evaluated considering type I and type II errors [42]. Type I errors were encountered when the PC scores of the blood plasma samples with antibodies to SARS-CoV-2 (IgG⁺-group) were not clustered together. Type II errors were seen when the PC scores of blood plasma samples without antibodies to SARS-CoV-2 (IgG⁻-group) were clustered with the IgG⁺-group scores.

The location of the samples in the coordinates of the first and second principal components does not show significant differences in the composition of the analyzed data (Figure 4). The differences are manifested only in the higher principal components. The greatest effect on the formation of lower principal components is made by the presence of fibrins contained in the plasma, which have a maximum absorption in the wavenumber range of 1600–1560 cm⁻¹. To reduce the overlap of the two groups, a narrower spectral range of 1680–1489 cm⁻¹ was chosen.

Figure 4 demonstrates that the minimum number of type I and type II errors (i.e. maximum grouping within groups and minimum overlap between two groups) is observed in the PC3–PC5 coordinates.

The scores for a sample of IR spectra of patients with antibodies to SARS-CoV-2 and without antibodies in the PC3–PC5 axes are shown in Figure 5a. The loadings of the principal components were calculated for centered and scaled data of the second derivative spectra. The loads for the PC4 and PC5 components are shown in Figure 5b. The highest values of the loadings in the negative region shift the coordinates of the sample counts to the negative region as much as possible, the positive values of the loadings—to the positive one.

Thus, the separation of the sample into two groups at axes principal component PC3–PC5 depends on the loading impact on the coordinates of a point at different wavenumbers. For samples corresponding to patients with antibodies to SARS-CoV-2, the greatest contribution

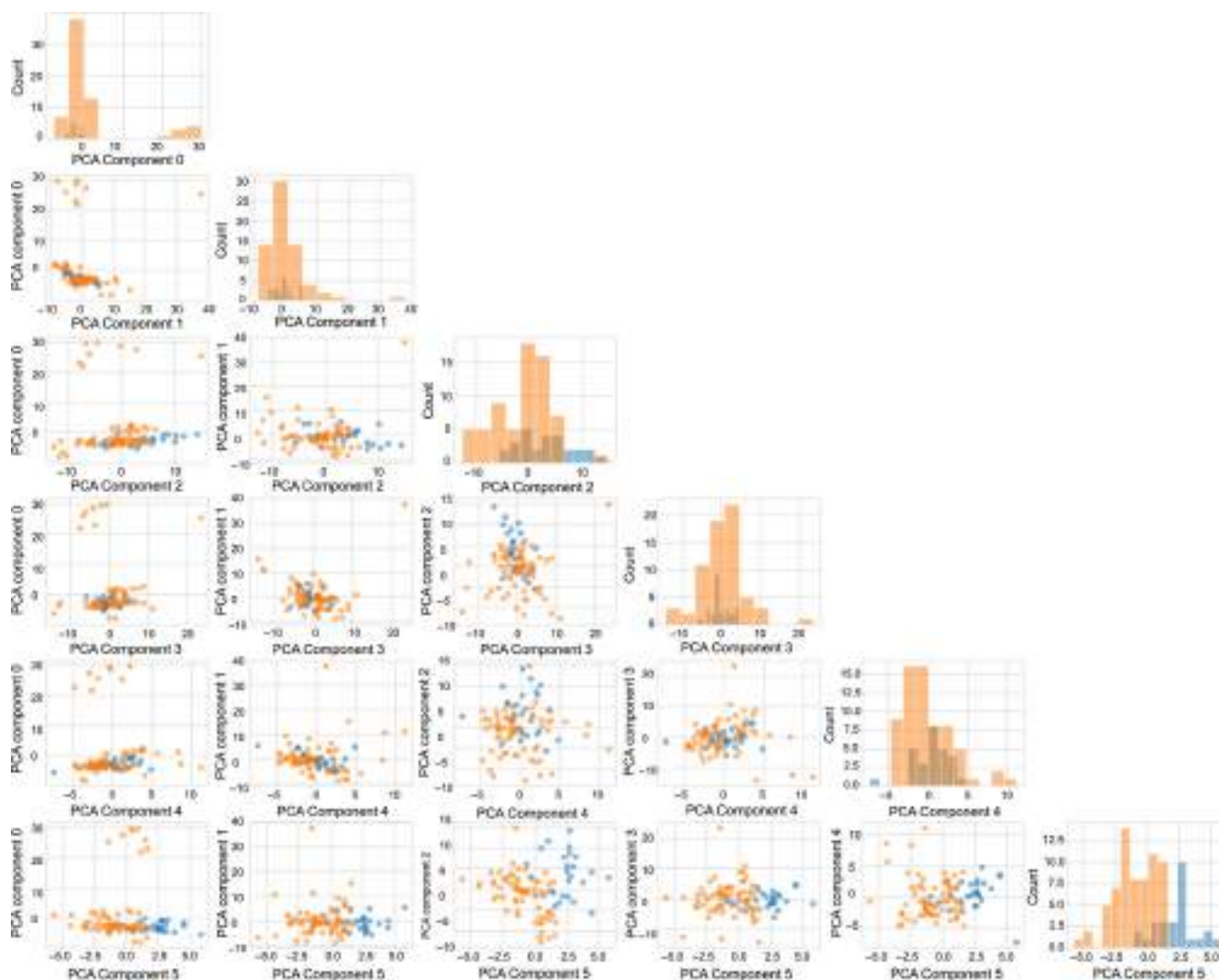


FIGURE 4 PCA result for two groups—control and recovered COVID-19 patients.

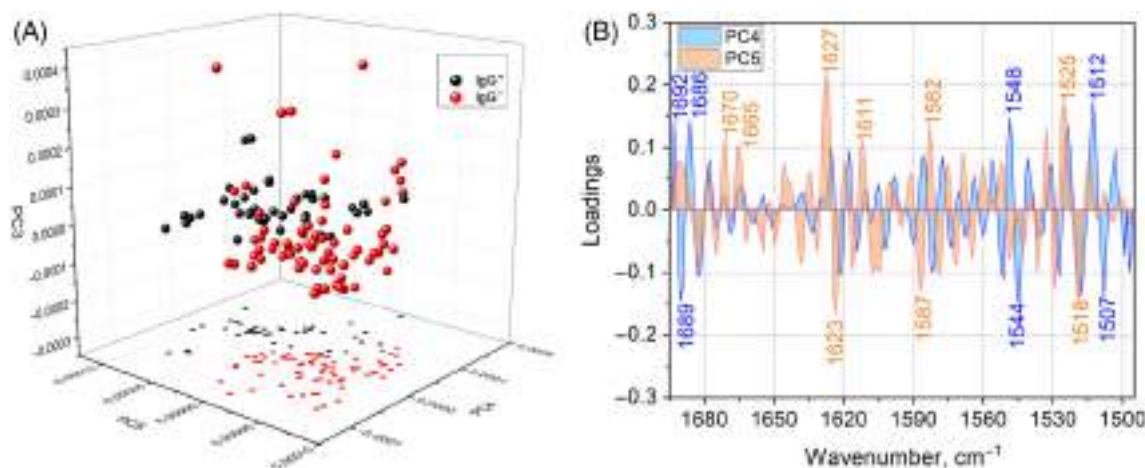


FIGURE 5 PCA scores plot of PC3 versus PC4 versus PC5 (a) in the 1680–1489 cm^{-1} region. Black dots represent the samples with antibodies to SARS-CoV-2 (IgG^+) and red dots the without antibodies (IgG^-) (the control group). Loading plot of PC4 and PC5 (b) in the 1680–1489 cm^{-1} region.

to the coordinates of the points is made by positive values of loadings calculated for PC4 at wavenumbers 1512, 1548, 1614, 1686 and 1692 cm^{-1} and positive values of loadings calculated for PC5 at wavenumbers 1525, 1582, 1611, 1627, 1670 cm^{-1} . For samples corresponding to patients without antibodies to SARS-CoV-2, the largest contribution to the coordinates of the points is made by the negative values of loadings calculated for PC4 at wavenumbers 1512, 1689 and 1692 cm^{-1} and positive values of loadings calculated for PC5 at wavenumbers 1525, 1627, 1670 cm^{-1} . Thus, the loading plots show that the main contribution to this difference is made by the frequency's characteristic of β -sheet structures, which are the main elements of immunoglobulins.

It is known that FTIR spectroscopy provides information on proteins, lipids and other components in serum, but in a more comprehensive and macroscopic view. Since proteins predominate in human serum, and albumin (about 70% of serum by mass) and IgG (14%) predominate in proteins, it can be assumed that changes in amide I are closely related to two types of proteins. HSA is predominated by α -helix and Ig by the β -sheet. The increase in Ig levels and decreases in albumin levels in the sera of patients with COVID-19, have been proved by a lot of reports. The IgG level in the patient sera elevates several times after the onset of COVID-19 [43–45]. As the loading plots obtained by the analysis of the principal components show, the main contribution to the differentiation of the two groups is made by the loads at frequencies characteristic of α -helical conformations (1665 cm^{-1}) and β -sheet conformations (1617, 1627, 1686, 1692 cm^{-1}).

Thus, multivariate and statistical analysis made it possible to assess the presence of seroconversion to SARS-CoV-2 using infrared spectroscopy. The spectrum

of the second derivative can increase the separation of overlapping bands and is thus more powerful than the original spectrum. This finding shows that multivariate methods hold promise for differentiating recovered COVID-19 patients from healthy controls.

3.3 | A study of protein aggregation in blood plasma samples from recovered COVID-19 patients

Infection with coronavirus-2 (SARS-CoV-2)/COVID-19 severe acute respiratory syndrome leads to the development of acute respiratory distress syndrome (ARDS). ARDS and associated inflammatory conditions in COVID-19 can lead to additional physiological abnormalities, including long-term health problems related not only to the respiratory system, but also to the heart and the nervous system. In a couple of recent papers, the authors hypothesized that some of these long-term complications may be related to COVID-19-induced protein aggregation [46, 47].

In a series of studies, it was shown that FTIR spectroscopy can be successfully used for the detection of protein aggregation [48–50]. Knowing this, we investigated the components of the secondary structure of the sum of proteins that make up human blood plasma to detect intermolecular β -sheets representing amyloid aggregates.

As a result of studies carried out over the past few years, a consensus has been reached regarding the use of many IR components in the field of amide I [51–54]. In general, the bands (in H_2O) in the 1643–1615 and 1692–1697 cm^{-1} regions are assigned to the β -sheet/extended conformation, 1647–1654 cm^{-1} to disordered structures,

1651–1663 cm^{-1} to loops, 1653–1660 cm^{-1} to α -helices and 1663–1695 cm^{-1} to turns. Amide I peak fit analysis has been shown to provide an accurate analysis of the secondary structure of proteins [48, 55], indicating that the procedure does not adversely affect the secondary structure of most proteins.

For blood plasma for two groups, the secondary structure of protein components was calculated (Figure 6) by the method of approximation (deconvolution) by Gaussian curves of the second derivatives of the subtraction spectra [56]. The results of deconvolution of the second derivatives of the IR spectra of blood plasma for the groups who have had COVID-19 patients and healthy donors are presented in Table 3.

As can be seen from Table 3, the average values of the components of the secondary structure of proteins for the two groups differ; however, statistically significant differences are only the ones between the intermolecular β -sheets for the group of recovered COVID-19 patients and controls.

Thus, based on the ANOVA test and the deconvolution of the second derivatives of the IR spectra, it can be concluded that the group of recovered COVID-19 patients is characterized by a slight increase in the proportion of

aggregated protein in the blood plasma, which may confirm the assumptions about the possibility of the formation of amyloid fibrils in the course of disease.

3.4 | Differentiate COVID-19 from Normal controls and sepsis

To exclude the association of the revealed differences between the previous two groups of samples (healthy and recovered COVID-19 patients) with post-COVID-19 inflammatory syndrome, plasma samples with confirmed sepsis were used, as a clinical condition with the most pronounced systemic inflammatory response. The study included 40 such samples to assess the effectiveness of the chemometric method.

Figure 7 shows the average IR spectrum with standard deviation for the control group, the group with antibodies against SARS-CoV-2 and sepsis. Differences are observed in the areas of amide A, amide I and amide III (Figures 7 and 8).

Compared to healthy donors and donors who have recovered from COVID-19, the spectra of blood plasma of patients with sepsis are distinguished by a greater

FIGURE 6 Examples of deconvolution of the second derivatives of IR spectra of blood plasma, a recovered COVID-19 patient (a) and a healthy donor (b)

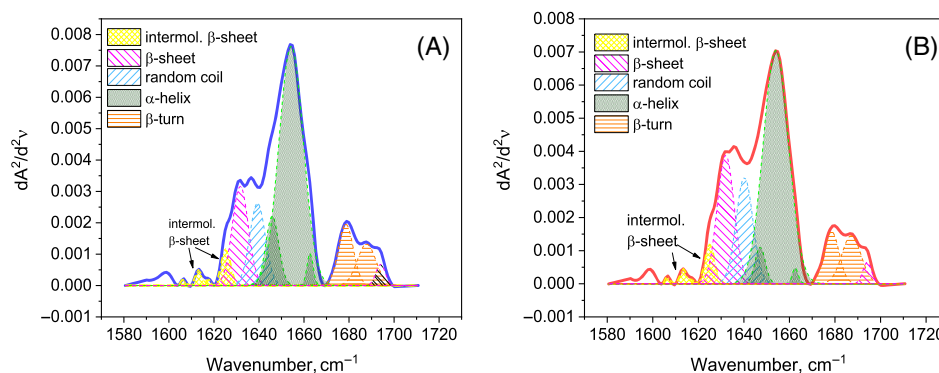


TABLE 3 Secondary structure of proteins that make up blood plasma recovered COVID-19 patients and the control group.

Component of secondary structure of proteins	Group	Mean	SD	SEM	Median	<i>p</i>
Intermol. β -sheet	IgG ⁺	1.70	0.44	0.08	1.58	0.040
	IgG [−]	1.48	0.38	0.07	1.49	
β -sheet	IgG ⁺	18.61	2.99	0.54	18.09	0.141
	IgG [−]	17.37	3.43	0.62	16.79	
Random coil	IgG ⁺	11.87	2.21	0.39	12.29	0.809
	IgG [−]	12.33	1.58	0.30	12.03	
α -helix	IgG ⁺	55.99	2.88	0.52	55.86	0.415
	IgG [−]	56.59	2.74	0.50	57.11	
β -turn	IgG ⁺	12.01	3.06	0.54	13.21	0.343
	IgG [−]	12.19	2.87	0.54	13.12	

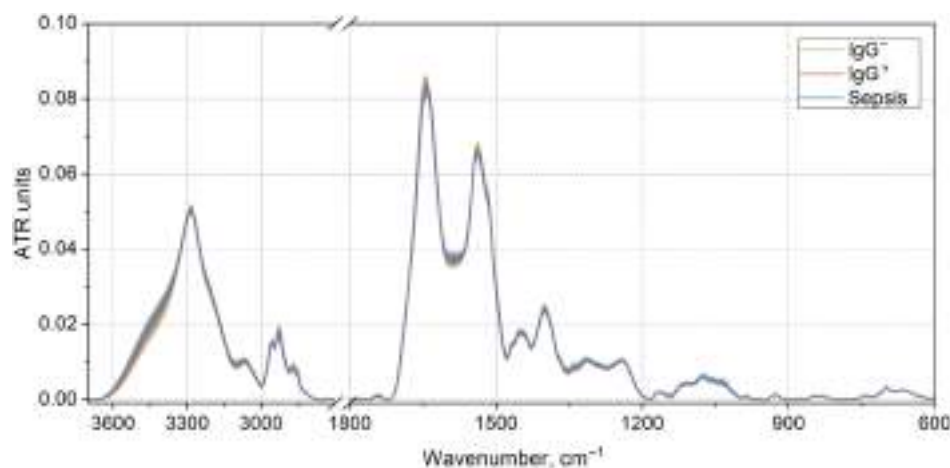


FIGURE 7 Average IR spectra of a sample of blood plasma with antibodies to SARS-CoV-2 (IgG^{\pm}), without antibodies (IgG^{-}), sepsis with standard deviation.

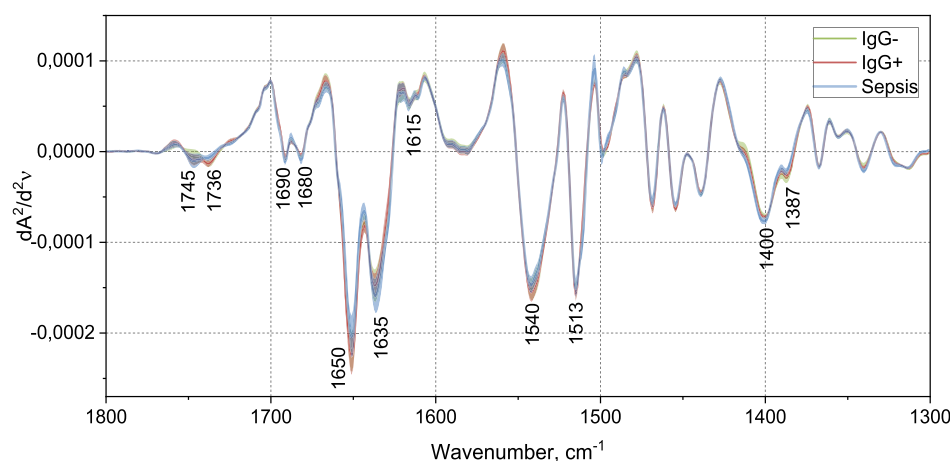


FIGURE 8 Average second derivatives of IR spectra of blood plasma groups with antibodies to COVID-19 (IgG^{+}), without antibodies (IgG^{-}) and patients with sepsis with standard deviation.

TABLE 4 Classification in the informative range of wavenumbers of the second derivatives of IR spectra.

Classifier	Median f1 score on cross-validation	Mean f1 score on cross-validation	Test accuracy	Number of PCA components
Gaussian process	0.71	0.74 ± 0.08	0.72	6
Decision tree	0.86	0.80 ± 0.12	0.81	21
KNeighbors	0.89	0.87 ± 0.08	0.85	34
SVC	0.89	0.89 ± 0.08	0.88	20
Random forest	0.94	0.89 ± 0.08	0.79	44
LDA	0.88	0.89 ± 0.09	0.87	28
MLP classifier	0.89	0.90 ± 0.05	0.86	21
AdaBoost	0.84	0.82 ± 0.11	0.78	35

intensity of the C—H, C=O bands characteristic of lipids and an altered protein profile. In the plasma spectra of patients with sepsis, a decreased content of α -helical conformations of proteins at a frequency of 1651 cm^{-1} and an increased content of β -sheet conformations at a frequency of 1635 cm^{-1} are observed (Figure 8). This corresponds to an increased content of proteins with a predominantly beta-sheet conformation, for example,

C-reactive proteins (CRP), as well as fibrinogen, which has an absorption at 1580 cm^{-1} . Also noteworthy are the features at 1177 and 1744 cm^{-1} , which correspond to circulating triglyceride-rich lipoproteins and free fatty acids. An increased level of circulating lipoproteins has been described as “lipidemia” of sepsis [57].

Due to the great similarity of spectral profiles for the three groups, chemometric approaches were used to

FIGURE 9 Results of classification by PCA-LDA for three groups of samples in the range of 1750–650 cm^{-1} .

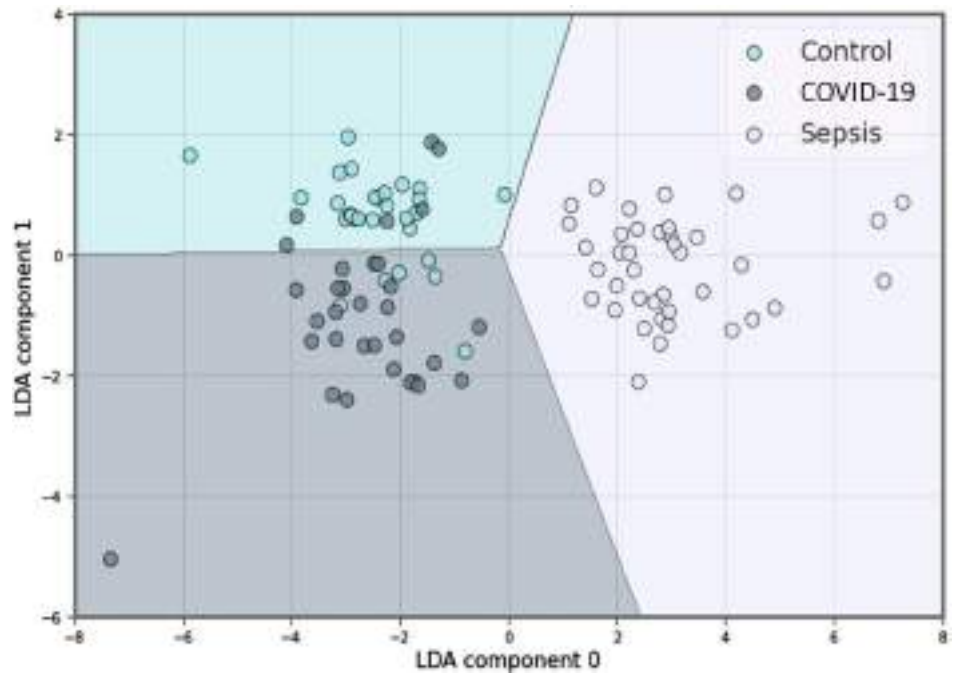
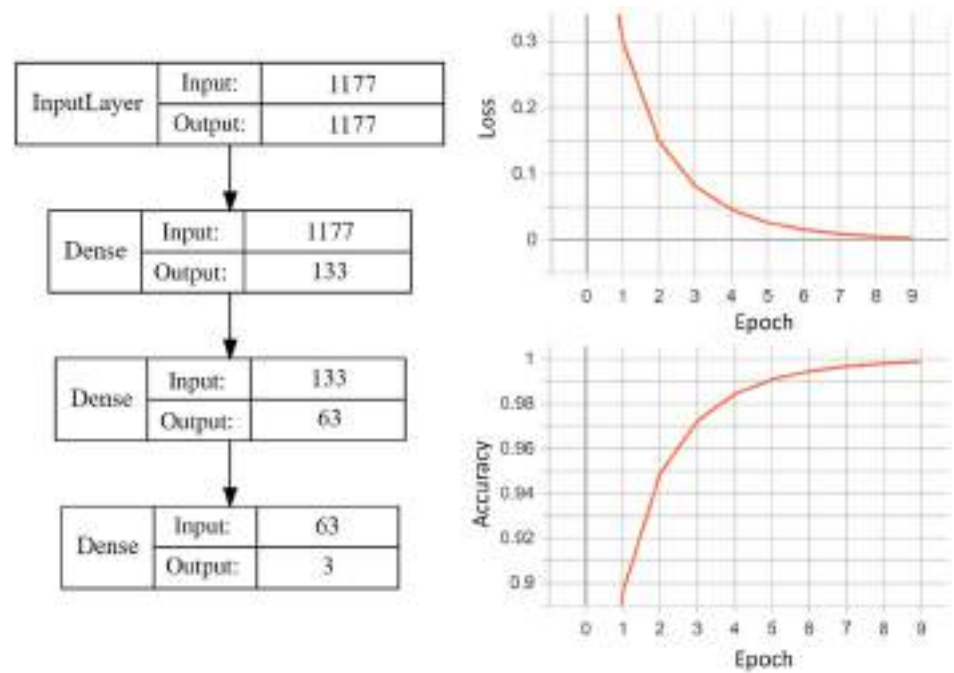


FIGURE 10 Artificial neural network (a)—Architecture, (b) dependence of loss function during training (c) dependence of accuracy during training.



determine the spectral characteristics responsible for class differentiation. For classification, the original dataset transformed by the principal component analysis was used. Well-known and efficient machine learning algorithms. To classify the three groups, a spectral range of 1785–650 cm^{-1} was selected. The results of using various classifiers are presented in Table 4. As can be seen, the best classification performance was obtained with the PCA-LDA, which showed an accuracy of 87% (Figures S3 and S4, Figure 9 and Table 4).

TABLE 5 Quality parameters calculated in the test set to classify healthy uninfected controls versus COVID-19 and sepsis-infected samples with neural network.

	Precision	Recall	F-score	G-score
Control	0.81	0.90	0.85	0.85
COVID-19	0.90	0.82	0.86	0.86
Sepsis	1.00	1.00	1.00	1.00
Accuracy	0.91			

TABLE 6 Comparison of classification results using PCA + LDA and ANN.

Classifier	Median f1-score on cross-validation	Mean f1-score on cross-validation	Test accuracy	Number of principal components
LDA	0.88	0.89 ± 0.09	0.87	28 PC
Artificial neural network	0.94	0.92 ± 0.07	0.91	1177 points of the spectrum

The neural networks were also used to increase the classification accuracy. The range $650\text{--}1785\text{ cm}^{-1}$ of the second derivative of the spectra was taken for analysis. This band corresponds to 1177 points, which are input values for the neural network. The neural network forms two hidden layers (Figure 10a): in the first layer there are 133 neurons with ReLU activation functions, in the second layer there are 63 neurons with ReLU activation functions, the third layer contains three neurons with a sigmoid activation function. Each of the three neurons of the output layer is responsible for its own class corresponding to COVID-19, sepsis or a healthy sample.

The loss function of categorical cross entropy and the “Adam” optimizer were chosen for training the neural network. The network was trained in 10 epochs, while showing the values given in Table 5, the training schedules are shown in Figure 10b,c.

Of all the models tested, the best classification performance was obtained with the PCA-LDA and neural network (Table 6) which showed good test accuracy (91% for neural network) and sensitivity (85%). The F and G scores show consistency, indicating that unbalanced class sizes did not affect classification performance.

4 | CONCLUSION

Taking into consideration the time required, the complexity of procedure and the detection of antibodies to perform COVID-19 FTIR spectroscopy in combination with multivariate analysis is a real tool for screening and identifying recovered COVID-19 patients. In this study, we used the ATR-FTIR spectroscopic method to elucidate changes in blood biochemical composition after recovery from COVID-19. The results showed mainly changes in the vibrational modes of proteins.

The PCA method shows that two groups, control and recovered COVID-19 patients, are well differentiated in the range of $1680\text{--}1490\text{ cm}^{-1}$, which indicates their difference in protein components. When classifying three groups (control, recovered COVID-19 patients, sepsis), the best sensitivity and specificity is shown by analysis in the range of $1750\text{--}650\text{ cm}^{-1}$. Chemometric methods such as PCA-LDA (87%) and ANN (91%) show greater accuracy.

The study shows that multivariate and statistical analysis provides an opportunity to assess the diagnosis of COVID-19 using second derivatives of infrared spectra and holds promise for differentiating recovered COVID-19 patients from healthy controls.

In addition, IR spectroscopy data allow us to assess the increased growth of aggregated proteins in the blood plasma of patients who have had COVID-19, which confirms modern ideas about the possibility of the formation of amyloid fibrils after a previous illness.

It is important to note that this method is fast and does not require labeling, and its use on a large scale may become possible in the future. Thus, the research results suggest that the IR spectroscopy method used in conjunction with chemometric methods has high potential in the mass diagnosis of the presence of immunity to SARS-CoV-2.

AUTHOR CONTRIBUTIONS

Boris Y. Karas: Formal analysis; data curation; writing—original draft preparation. **Vera E. Sitnikova:** Conceptualization; methodology; formal analysis; visualization; writing—original draft preparation; project administration. **Daria S. Potapova:** Formal analysis; data curation. **Tatiana N. Nosenko:** Conceptualization; formal analysis; data curation; methodology; investigation. **Vladimir G. Dedkov:** Supervision; resources; writing—reviewing and editing. **Natalia A. Arsentieva:** ELISA; formal analysis; sample characterization. **Areg A. Totolian:** Supervision. **Natalia V. Gavrilenko:** Bio-banking of plasma samples. **Ivan S. Moiseev:** Supervision. **Mayya V. Uspenskaya:** Supervision; funding acquisition; writing—reviewing and editing.

CONFLICT OF INTEREST STATEMENT

There are no conflicts to declare.

DATA AVAILABILITY STATEMENT

The data that support the findings of this study are available from the corresponding author upon reasonable request.

ORCID

Vera E. Sitnikova  <https://orcid.org/0000-0003-4753-976X>

Tatiana N. Nosenko  <https://orcid.org/0000-0003-4159->

133X

Vladimir G. Dedkov  <https://orcid.org/0000-0002-5500-0169>

Natalia A. Arsentieva  <https://orcid.org/0000-0003-2490-308X>

Ivan S. Moiseev  <https://orcid.org/0000-0002-4332-0114>

Areg A. Totolian  <https://orcid.org/0000-0003-4571-8799>

Andrey V. Kajava  <https://orcid.org/0000-0002-2342-6886>

Mayya V. Uspenskaya  <https://orcid.org/0000-0003-2510-2639>

REFERENCES

- [1] (Website) Author, Short description or title, URL (accessed Month, Year).
- [2] P. Sinha, M. A. Matthay, C. S. Calfee, *JAMA Intern. Med.* **2020**, *180*, 1152.
- [3] D. Wang, B. Hu, C. Hu, *JAMA Intern. Med.* **2020**, *323*, 1061.
- [4] X. W. Xu, X. X. Wu, X. G. Jiang, *BMJ* **2020**, *368*, m606.
- [5] C. Rothe, M. Schunk, P. Sothmann, *N. Engl. J. Med.* **2020**, *19*, 970.
- [6] M. Yang, L. L. T. Huang, S. Li, M. Zhang, Y. Yang, Y. Jiang, X. Li, J. Yuan, Y. Liu, *Am. J. Respir. Crit. Care Med.* **2021**, *203*, 374.
- [7] H. Y. Chung, M. Jian Jr., C. K. Chang, J. C. Lin, K. M. Yeh, C. W. Chen, S. K. Chiu, Y. H. Wang, S. J. Liao, S. Y. Li, S. S. Hsieh, S. H. Tsai, C. L. Perng, J. R. Yang, M. T. Liu, F. Y. Chang, H. S. Shang, *Emerg. Microbes Infect.* **2021**, *10*, 161.
- [8] N. L. Hardy, P. M. Luethy, *J. Appl. Lab. Med.* **2021**, *6*, 1484.
- [9] E. A. Goncharova, V. G. Dedkov, A. S. Dolgova, I. S. Kassirov, M. V. Safonova, Y. Voytsekhovskaya, A. A. Totolian, *J. Med. Virol.* **2021**, *93*, 1694.
- [10] T. R. Shelite, A. C. Uscanga-Palomeque, A. Castellanos-Gonzalez, P. C. Melby, B. L. Travi, *J. Virol. Methods* **2021**, *296*, 114227.
- [11] J. Lee, S. Y. Kim, H. J. Huh, N. Kim, H. Sung, H. Lee, K. H. Roh, T. S. Kim, K. H. Hong, *Ann. Lab. Med.* **2021**, *41*, 588.
- [12] S. Savini, D. Monaco, C. Turci, S. Ursino, C. Matera, R. Marchini, T. DiGiovanni, E. Ciambella, V. Iannucci, G. Quintavalle, *Ann. Ig.* **2021**, *33*, 518.
- [13] E. J. Nilles, E. W. Karlson, M. Norman, T. Gilboa, S. T. Fischinger, C. Atyeo, G. Zhou, C. H. L. Bennett, N. V. Tolan, K. Oganezova, D. R. Walt, G. Alter, D. P. Simmons, P. Schur, P. Jarolim, A. Woolley, L. R. Baden, *J. Appl. Lab. Med.* **2021**, *6*, 1561.
- [14] S. E. Larsen, B. J. Berube, T. Pecor, E. Cross, B. P. Brown, B. Williams, E. Johnson, P. Qu, L. Carter, S. Wrenn, E. Kepl, C. Sydemann, N. P. King, S. L. Baldwin, R. N. Coler, *bioRxiv* **2021**, *499*, 113160.
- [15] K.-Y. Su, W.-L. Lee, *Cancers* **2020**, *12*, 115.
- [16] A. Sala, D. J. Anderson, P. M. Brennan, H. J. Butler, J. M. Cameron, M. D. Jenkinson, C. Rinaldi, A. G. Theakstone, M. J. Baker, *Cancer Lett.* **2020**, *477*, 122.
- [17] V. E. Sitnikova, M. A. Kotkova, T. N. Nosenko, T. N. Kotkova, D. M. Martynova, M. V. Uspenskaya, *Talanta* **2020**, *214*, 120857.
- [18] J. Titus, C. Filfili, J. K. Hilliard, J. A. Ward, A. Unil-Perera, *Appl. Phys. Lett.* **2014**, *104*, 243705.
- [19] K. A. Chan, S. G. Kazarian, *Chem. Soc. Rev.* **2016**, *45*, 1850.
- [20] C. M. Orphanou, *Forensic Sci. Int.* **2015**, *252*, e10.
- [21] L. Zhang, M. Xiao, Y. Wang, Y. Siqi Peng, D. Z. Chen, D. Zhang, Y. Guo, X. Wang, H. Luo, Q. Zhou, X. Yingchun, *Anal. Chem.* **2021**, *19*, 2191.
- [22] A. Banerjee, A. Gokhale, R. Bankar, V. Palanivel, A. Salkar, H. Robinson, J. S. Shastri, S. Agrawal, G. Hartel, M. M. Hill, S. Srivastava, *Anal. Chem.* **2021**, *93*, 10391.
- [23] B. R. Wood, K. Kochan, D. E. Bedolla, N. Salazar-Quiroz, S. L. Grimley, D. Perez-Guaita, M. J. Baker, J. Vongsvivut, M. J. Tobin, K. R. Bamberg, D. Christensen, S. Pasricha, A. K. Eden, A. Mclean, S. Roy, J. A. Roberts, J. Druce, D. A. Williamson, J. McAuley, M. Catton, D. F. J. Purcell, D. I. Godfrey, P. Heraud, *Am. Ethnol.* **2021**, *60*, 17102.
- [24] V. G. Barauna, M. N. Singh, L. L. Barbosa, W. D. Marcarini, P. F. Vassallo, J. G. Mill, R. Ribeiro-Rodrigues, L. C. G. Campos, P. H. Warnke, F. L. Martin, *Anal. Chem.* **2021**, *93*, 2950.
- [25] M. H. C. Nascimento, W. D. Marcarini, G. S. Folli, W. G. da Silva Filho, L. L. Barbosa, E. H. de Paulo, P. F. Vassallo, J. G. Mill, V. G. Barauna, F. L. Martin, E. V. R. de Castro, W. Romão, P. R. Filgueiras, *Anal. Chem.* **2022**, *94*, 2425.
- [26] S. T. Kazmer, G. Hartel, H. Robinson, R. S. Richards, K. Yan, S. J. VanHal, R. Chan, A. Hind, D. Bradley, F. Zieschang, D. J. Rawle, T. T. Le, D. W. Reid, A. Suhrbier, M. M. Hill, *Biomedicine* **2022**, *10*, 351.
- [27] D. L. Kitane, S. Loukman, N. Marchoudi, A. Fernandez-Galiana, F. Z. El Ansari, F. Jouali, J. Badir, J. L. Gala, D. Bertsimas, N. Azami, O. Lakbata, O. Moudam, R. Benhida, J. Fekkak, *Sci. Rep.* **2021**, *11*, 16740.
- [28] G. J. Vazquez-Zapien, A. Martinez-Cuazitl, M. Sanchez-Brito, R. J. Delgado-Macuil, C. Atriano-Colorado, F. Garibay-Gonzalez, V. Sanchez-Monroy, A. Lopez-Reyes, M. M. Mata-Miranda, *Cell* **2022**, *11*, 3884.
- [29] A. Y. Popova, E. B. Ezhlova, A. Mel'nikova, N. S. Bashketova, R. K. Fridman, L. V. Lyalina, V. S. Smirnov, I. G. Chkhindzheriya, T. A. Grechaninova, K. A. Agapov, N. A. Arsent'eva, N. A. Bazhenova, O. K. Batsunov, E. M. Danilova, E. V. Zueva, D. V. Komkova, R. N. Kuznetsova, N. E. Lyubimova, A. N. Markova, I. V. Khamitova, V. I. Lomonosova, V. V. Vetrov, A. M. Milichkina, V. G. Dedkov, A. A. Totolyan, *Probl. Osobo Opasnykh Infektsii* **2020**, *3*, 124.
- [30] A. Rhodes, L. E. Evans, W. Alhazzani, M. M. Levy, M. Antonelli, R. Ferrer, A. Kumar, J. E. Sevransky, C. L. Sprung, M. E. Nunnally, B. Rochweg, G. D. Rubinfeld, D. C. Angus, D. Annane, R. J. Beale, G. J. Bellinghan, G. R. Bernard, J. D. Chiche, C. Coopersmith, D. P. DeBacker, C. J. French, S. Fujishima, H. Gerlach, J. L. Hidalgo, S. M. Hollenberg, A. E. Jones, D. R. Karnad, R. M. Kleinpell, Y. Koh, T. C. Lisboa, F. R. Machado, J. J. Marini, J. C. Marshall, J. E. Mazuski, L. A. McIntyre, A. S. McLean, S. Mehta, R. P. Moreno, J. Myburgh, P. Navalesi, O. Nishida, T. M. Osborn, A. Perner, C. M. Plunkett, M. Ranieri, C. A. Schorr, M. A. Seckel, C. W. Seymour, L. Shieh, K. A. Shukri, S. Q. Simpson, M. Singer, B. T. Thompson, S. R. Townsend, T. V. Poll, J. L. Vincent, W. J. Wiersinga, J. L. Zimmerman, R. P. Dellinger, *Intensive Care Med.* **2017**, *43*, 304.
- [31] C. L. M. Morais, K. M. G. Lima, *Chemom. Intell. Lab. Syst.* **2017**, *70*, 1.
- [32] F. Pedregosa, G. Varoquaux, A. Gramfort, V. Michel, B. Thirion, O. Grisel, M. Blondel, P. Prettenhofer, R. Weiss, V.

- Dubourg, J. Vanderplas, A. Passos, D. Cournapeau, M. Brucher, M. Perrot, E. Duchesnay, *J. Mach. Learn. Res.* **2011**, 12, 2825.
- [33] J. Trevisan, P. P. Angelov, P. L. Carmichael, A. D. Scott, F. L. Martin, *Analyst* **2012**, 137, 3202.
- [34] R. L. Somorjai, B. Dolenko, R. Baumgartner, *Bioinformatics* **2003**, 19, 1484.
- [35] Z. Movasaghi, S. Rehman, I. Rehman, *Appl. Spectrosc. Rev.* **2008**, 43, 134.
- [36] M. J. Baker, J. Trevisan, P. Bassan, R. Bhargava, H. J. Butler, K. M. Dorling, P. R. Fielden, S. W. Fogarty, N. J. Fullwood, K. A. Heys, C. Hughes, P. Lasch, P. L. Martin-Hirsch, B. Obinaju, G. D. Sockalingum, J. Sulé-Suso, R. J. Strong, M. J. Walsh, B. R. Wood, P. Gardner, F. L. Martin, *Nat. Protoc.* **2014**, 9, 1771.
- [37] F. L. Martin, J. G. Kelly, V. Llabjani, P. L. Martin-Hirsch, I. I. Patel, J. Trevisan, N. J. Fullwood, M. J. Walsh, *Nat. Protoc.* **2010**, 5, 1748.
- [38] N. Dieter, *Appl. Spectrosc. Rev.* **2001**, 36, 239.
- [39] R. Eccles, *Lancet Infect. Dis.* **2015**, 5, 718.
- [40] R. Wölfel, V. M. Corman, W. Guggemos, M. Seilmaier, S. Zange, M. A. Müller, D. Niemeyer, T. C. Jones, P. Vollmar, C. Rothe, M. Hoelscher, T. Bleicker, S. Brünink, J. Schneider, R. Ehmann, K. Zwirgmaier, C. Drosten, C. Wendtner, *Nature* **2020**, 581, 465.
- [41] D. Wu, T. Shu, X. Yang, J.-X. Song, M. Zhang, C. Yao, W. Liu, M. Huang, Y. Yu, Q. Yang, T. Zhu, J. Xu, J. Mu, Y. Wang, H. Wang, T. Tang, Y. Ren, Y. Wu, S.-H. Lin, Y. Qiu, D.-Y. Zhang, Y. Shang, X. Zhou, *Natl. Sci. Rev.* **2020**, 7, 1157.
- [42] S. Assi, I. Robertson, T. Coombs, J. McEachran, K. Evans, *Spectroscopy* **2019**, 34, 46.
- [43] B. Zhang, X. Zhou, C. Zhu, Y. Song, F. Feng, Y. Qiu, J. Feng, Q. Jia, Q. Song, B. Zhu, J. Wang, *Front. Mol. Biosci.* **2020**, 7, 157.
- [44] N. Chen, M. Zhou, X. Dong, J. Qu, F. Gong, Y. Han, Y. Qiu, J. Wang, Y. Liu, Y. Wei, J. Xia, T. Yu, X. Zhang, L. Zhang, *Lancet* **2019**, 395, 507.
- [45] N. Sinha, A. K. Thakur, *Trends Microbiol.* **2021**, 7, 1157.
- [46] S. A. Semerdzhiev, M. Fakhree, I. Segers-Nolten, C. Blum, M. A. E. Claessens, *ACS Chem. Neurosci.* **2022**, 13, 143.
- [47] E. Pretorius, C. Venter, G. J. Laubscher, P. J. Lourens, J. Steenkamp, D. B. Kell, *Cardiovasc. Diabetol.* **2020**, 19, 193.
- [48] D. Usoltsev, V. Sitnikova, A. Kajava, M. Uspenskaya, *Biomolecules* **2019**, 9, 359.
- [49] A. Stirpe, M. Pantusa, B. Rizzuti, M. P. De Santo, L. Sportelli, R. Bartucci, R. Guzzi, *Int. J. Biol. Macromol.* **2016**, 92, 1049.
- [50] B. Shivu, S. Seshadri, J. Li, K. A. Oberg, V. N. Uversky, A. L. Fink, *Biochemistry* **2013**, 52, 5176.
- [51] H. H. Kampinga, E. Muller, J. F. Brunsting, L. Heine, A. W. Konings, R. D. Issels, *Int. J. Hyperth.* **1993**, 9, 89.
- [52] A. E. Kabakov, V. L. Gabai, *Experientia* **1993**, 49, 706.
- [53] A. Laszlo, W. Wright, J. Roti, L. Roti, *J. Cell. Physiol.* **1992**, 151, 519.
- [54] N. J. Harrick, *Internal Reflection Spectroscopy*, Wiley Interscience, New York **1967**.
- [55] E. Goormaghtigh, V. Raussens, J. M. Ruyschaert, *Biochim. Biophys. Acta* **1999**, 1422, 105.
- [56] H. Yang, S. Yang, J. Kong, A. Dong, S. Yu, *Nat. Protoc.* **2015**, 10, 382.
- [57] J. I. Gallin, D. Kaye, W. M. O'Leary, *N. Engl. J. Med.* **1969**, 281, 1081.

SUPPORTING INFORMATION

Additional supporting information can be found online in the Supporting Information section at the end of this article.

How to cite this article: B. Y. Karas, V. E. Sitnikova, T. N. Nosenko, V. G. Dedkov, N. A. Arsentieva, N. V. Gavrilenko, I. S. Moiseev, A. A. Totolian, A. V. Kajava, M. V. Uspenskaya, *J. Biophotonics* **2023**, 16(7), e202200166. <https://doi.org/10.1002/jbio.202200166>